

---

# VISUALIZING DEEP NEURAL NETWORKS WITH TOPOGRAPHIC ACTIVATION MAPS

---

Andreas Krug, Raihan Kabir Ratul, Sebastian Stober

Artificial Intelligence Lab  
Otto-von-Guericke-University Magdeburg  
39106 Magdeburg, Germany

## ABSTRACT

Machine Learning with Deep Neural Networks (DNNs) has become a successful tool in solving tasks across various fields of application. The success of DNNs is strongly connected to their high complexity in terms of the number of network layers or of neurons in each layer, which severely complicates to understand how DNNs solve their learned task. To improve the explainability of DNNs, we adapt methods from neuroscience because this field has a rich experience in analyzing complex and opaque systems. In this work, we draw inspiration from how neuroscience uses topographic maps to visualize the activity of the brain when it performs certain tasks. Transferring this approach to DNNs can help to visualize and understand their internal processes more intuitively, too. However, the inner structures of brains and DNNs differ substantially. Therefore, to be able to visualize activations of neurons in DNNs as topographic maps, we research techniques to layout the neurons in a two-dimensional space in which neurons of similar activity are in the vicinity of each other. In this work, we introduce and compare different methods to obtain a topographic layout of the neurons in a network layer. Moreover, we demonstrate how to use the resulting topographic activation maps to identify errors or encoded biases in DNNs or data sets. Our novel visualization technique improves the transparency of DNN-based algorithmic decision-making systems and is accessible to a broad audience because topographic maps are intuitive to interpret without expert-knowledge in Machine Learning.

**Keywords** neural networks · deep learning · model evaluation · explainable AI · visualization · topographic maps

## 1 Introduction

Machine Learning with Deep Neural Networks (DNNs) is a popular tool and highly successful in solving tasks in many fields of application [48]. However, the associated increase of DNN complexity in terms of the number of network layers or of neurons in each layer severely complicates the understanding of how DNNs solve their learned task [52]. To improve the explainability of DNNs, we transfer methods for analyzing complex and opaque systems from the field of neuroscience, which has been studying the brain over decades. In this work, we focus on adapting how brain activity is typically visualized as a topographic map. For example, brain activity recorded through Electroencephalography (EEG) measurements [28] is represented as a top view of the head with a superimposed topographic map of neural activity [29]. Adapting this approach to be applicable to DNNs can help to visualize and understand their internal processes more intuitively, too. However, in contrast to the brain, DNNs typically do not have an informative order of neurons because there are no connections between neurons within the same layer. Therefore, to be able to visualize activations of neurons in DNNs as topographic maps, we research techniques to layout the neurons in a two-dimensional space in which neurons of similar activity are in the vicinity of each other. The idea of introducing a topographic neuron layout in artificial neural networks is not novel. Self-Organizing Maps (SOMs) [22] follow a similar motivation and already constrain the neurons to form a topographical layout during training. However, traditional SOMs are only shallow neural networks and more recent approaches on training deep SOMs [26] have not gained popularity yet. Most Deep Learning (DL) models that are used in practice are implemented without a topographical layout of the neurons. Our

aim is to provide the possibility to create a topographic layout visualization for any DNN, particularly those that are already trained and potentially deployed in the real world.

In this work, we introduce and compare different methods to obtain a topographic layout of neurons in the same layer of a DNN. Moreover, we demonstrate how to use the resulting visualization as topographic maps to analyze DNNs. To this end, we show how to visually compare the activations of DNN-based classifiers between different classes and how to derive potential reasons for erroneous predictions from this comparison. In addition, we demonstrate how to visualize biases that are encoded in the representations of pre-trained DNN models. Our novel visualization technique improves the transparency of algorithmic decision-making systems that use DNNs. In addition, our visual representation of complex activation patterns of DNNs is interpretable without expert-knowledge in Machine Learning and is therefore accessible to a broad audience. In this work, we particularly focus on the visualization of internal representations of DNNs. Fixing models or mitigating biases is out of the scope of this work, but detecting errors with our technique allows to apply existing strategies for improving the model in a more targeted manner.

## 2 Related Work

### 2.1 Deep Neural Network Analysis

Getting insight into the internal structures and processes of trained DNNs is crucial because such models work as black-boxes [52]. Consequently, researchers proposed various methods for visualizing and analyzing DNNs. These approaches are often best suitable for image data [53, 41, 4] because input images and the corresponding model explanations are visually interpretable by a human. Popular DNN explanation techniques aim to visualize the learned features of the model [52, 10, 32], highlighting prediction-relevant values in the input [10, 44, 53] or analyzing the learned representations [3, 18, 31, 23].

#### 2.1.1 Feature Visualization

Feature visualization aims to explain the internal structures of a trained DL model. The connection weights between the neurons of a DNN are the trained parameters of the model. Therefore, inspecting these weights can help to understand which patterns the trained model responds to. In Multi-Layer Perceptrons (MLPs), the weight values of connections from the input to a single neuron in the first hidden layer can be directly visualized as a heat map [36]. For two-dimensional data like images, the resulting heat maps are two-dimensional images, too. For Convolutional Neural Networks (CNNs), plotting the weights is not a useful visualization because these models apply weights as convolution operations with filters that are typically very small, for example,  $3 \times 3$ . Hence, the visualization of the weights is a tiny image and difficult to interpret.

Alternatively, CNN features can be visualized by plotting the feature maps, that is, all activation values of the same convolutional filter. However, feature maps only show which parts of the input the filter responds to but do not visualize the detected pattern [52]. To further investigate which pattern is detected by the convolutional filter, an artificial input which maximally activates this filter can be created through optimization [52, 10, 32]. Using a data example or random values as initial input, its values are updated by an optimization algorithm to maximize the activation values of the feature map of interest. This approach for CNN feature visualization is also referred to as Activation Maximization (AM). If inputs are optimized without constraints, they can appear unrealistic to a human and hence be hard to interpret. Therefore, AM is typically performed with regularization techniques that penalize unnatural inputs [32]. While regularization makes optimized inputs more realistic, it can decrease the faithfulness of the pattern visualization if the optimization overemphasizes the similarity of the optimized input to natural data.

#### 2.1.2 Saliency Maps

To explain the output of a DL model for an individual input example, the influence of input values on the output can be quantified. Attribution techniques aim to compute the relevance of each input value for the output of the DNN [10, 44, 53, 46, 41, 19, 40]. The relevance values are then visualized as a superimposed heat map on the input. Commonly, the relevance heat maps are referred to as saliency maps [44]. Due to the complexity of DNNs, it is infeasible to compute the relevance values exactly. Therefore, various attribution techniques have been suggested that, for example, compute gradients of the output with respect to the input values [10], combine gradient information with activation values [41] or decompose the output [4]. Saliency maps are only interpretable if the input data are visually interpretable themselves because the saliency values are superimposed on the input. Hence, saliency maps are particularly suitable for image data and data that can be interpreted as image, for example, audio data as spectrograms [5, 49, 38]. Attribution techniques are convenient due to the ease of visually interpreting them but have disadvantages, as well. Because saliency maps are computed for individual examples only, it is difficult to draw conclusions about

how the model performs its task in general. Moreover, some attribution techniques can be misleading because their relevance computation is not strongly enough related to the output [1, 35, 45].

### 2.1.3 Data Representation Analysis

To investigate how the DNN processes the input data in general, the model-internal representations of the data can be analyzed. To this end, the hidden layer activations for the complete data set or a subset of it are computed and further evaluated in-depth. For example, training linear models to classify the representations in a hidden layer indicates how well particular properties are encoded in this layer. The classification targets of the linear models can be the targets of the DNN itself [3] or any user-defined property by providing groups of inputs [18]. A more general approach than investigating linear separability is to analyze the representational similarity between groups of related examples. Previous work used Principal Component Analysis (PCA) [11], Canonical Correlation Analysis (CCA) [31] or clustering techniques [33, 23] to find co-activated neurons or to compare representations of different groups of examples. Our introduced technique aims to analyze activations, as well, but in contrast to existing approaches, it allows to compare high-dimensional representations by visual inspection. Explaining DNNs by investigating their activations only gives insight into model behavior for groups that are contained in the used test data.

## 2.2 Bias detection in DNNs

DNNs are prone to reproducing or emphasizing biases that are contained in the data used to train them. Different approaches to detect and mitigate bias have been introduced. For example, Sweeney [47] shows racial discrimination in the online ad delivery by Google and Bolukbasi et al. [6] debias commonly used word embeddings. More recently, researchers investigate biases in modern transformer-based models like BERT [8], for example focusing on gender bias [25] or ethnic bias [2]. Discrimination in facial recognition algorithms is evaluated by Buolamwini and Gebru [7] and they introduced the Gender Shades data set with a balanced distribution of gender and skin type. Similarly, Karkkainen and Joo [16] introduced the Fair Face data set which is balanced for gender, race and age categories. In this work, we perform racial bias detection as an exemplary use case of our novel visualization technique. Different to Buolamwini and Gebru [7] or Karkkainen and Joo [16], who investigate bias in the output and the performance of algorithmic decision systems, we focus on bias in the representations of the individual layers of a DNN.

## 3 Methods

In this section, we describe our proposed pipeline to compute the topographic activation maps. This includes obtaining the hidden layer representations of groups of examples, computing the layout of the topographic maps and visualizing the activations according to the layout. A visual abstract of the pipeline is shown in Figure 1. The implementation is publicly available on <https://github.com/andreaskrug/ANN-topomaps>.

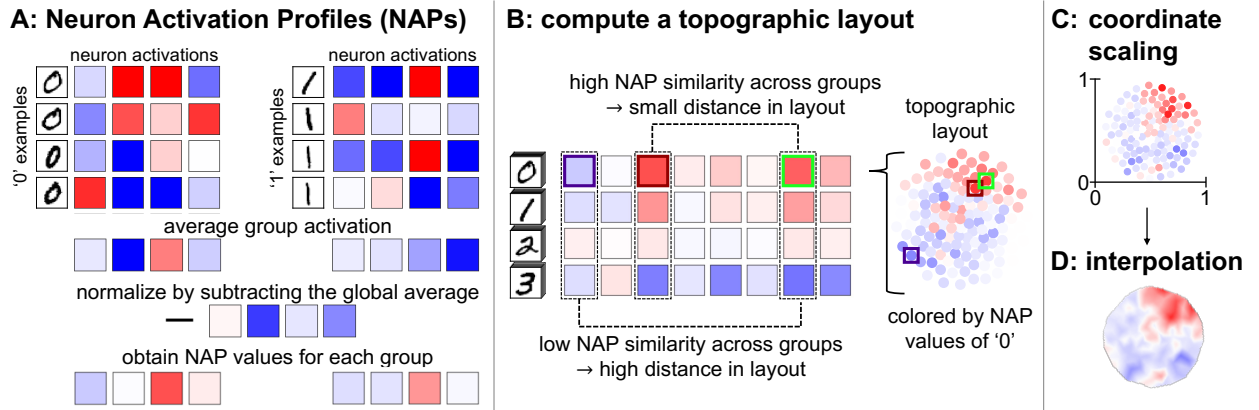


Figure 1: Visual summary of the computation of topographic activation maps. A: obtain NAPs to characterize the DNN activations for the groups of interest. B: compute a layout in which similarly activated neurons are in the vicinity of each other. C: scale the coordinates in both dimensions to a range from 0 to 1. D: apply interpolation to achieve a continuous coloring.

### 3.1 Hidden Layer Representations

The topographic layout computation is based on neuron activation similarity. Hence, the initial step is to obtain values that describe the DNN activity for the groups of interest. A straight-forward strategy is to use the stacked DNN activations for multiple data examples. However, the computational effort is high because the dimensionality of the stacked activation values increases with the number of provided examples and the activations do not specifically represent the investigated groups. Therefore, we use an averaging approach with normalization, adapted from Krug et al. [23]. For each group, we compute the average activations in the layer of interest and normalize the result by subtracting the average activation over all groups (Figure 1A). For the layout computation, we stack the obtained values (Figure 1B) to obtain a  $N \times G$  matrix, where  $N$  and  $G$  denote the number of neurons and groups, respectively. Following the terminology by Krug et al. [23], we refer to the resulting matrix as the Neuron Activation Profile (NAP) of the layer. Different from the original NAP approach, we only use random subsets of examples from each investigated group to be able to efficiently apply our method to larger data sets. Moreover, we omit the authors' proposed alignment procedure because we only use image data sets in which the objects are already centered.

Neurons in CNNs are arranged as feature maps and neurons in the same feature map detect a common feature. Therefore, we characterize the feature map activations instead of each individual neuron. In CNNs, we average and normalize each feature map across the groups. Then, we flatten each averaged feature map of size  $w \times h$  to a  $w \times h$ -dimensional vector and stack the vectors of all groups. The resulting  $w \times h \times G$ -dimensional vector characterizes the activations of one feature map. Finally, the NAP of the layer is obtained by stacking these vectors for all feature maps, resulting in a  $N \times (w \times h \times G)$  matrix.

### 3.2 Topographic Map Layout

To compute the layout of the topographic maps, we distribute the neurons of a hidden layer in a two-dimensional space. In general, we aim to compute a layout in which neurons of similar activity are in the vicinity of each other (Figure 1B). While using the same layout for all groups, we aim for activation similarity of nearby neurons in each individual group.

#### 3.2.1 Self-Organizing Map (SOM)

We use the MiniSom<sup>1</sup> package for Python to compute a SOM [22] layout of the neurons based on their activations. For a layer of  $N$  neurons, we compute a square SOM with shape  $d \times d$  with  $d = \lfloor \sqrt{N} + 1 \rfloor$  such that there can potentially be one SOM position per neuron. We train the SOM for 10 epochs with the NAPs as training data and using the default parameters of the MiniSom package. Then, we assign each neuron the coordinate of the SOM position whose weights are most similar to the NAP values of the neuron. However, multiple neurons can match best to the same position in the trained SOM and hence will be indistinguishable in the layout. Therefore, for each set of neurons that share the same coordinate, we distribute the neurons uniformly on a circle centered at the coordinate assigned to the neurons. To ensure that the redistributed neurons are still closer to each other than to other neurons, considering that the SOM coordinates are integer-valued, we choose a circle radius of 0.2.

#### 3.2.2 Co-Activation Graph

The co-activation graph approach follows the idea of layouting a graph structure in which nodes and edges represent neurons and their activation similarity, respectively. We first compute the pairwise Cosine similarity of neurons according to their NAP values. We then create a graph with one node corresponding to each neuron. For each of the 7.5% most similar pairs of neurons, we draw an edge between the corresponding nodes in the graph. We empirically choose the distance threshold based on the connectedness of the graphs for several MLP models and layers. The resulting graph can have separated subsets of nodes, which leads to large gaps in the layout. To avoid these gaps, we further ensure that the entire graph is connected. To this end, we first identify all maximal subsets of nodes where a path exists between all nodes, called connected components. Then, we link each smaller connected component to the largest one by drawing an edge between the most similar pair of neurons out of the two components. Finally, we layout the connected graph with the force-directed Fruchterman Reingold algorithm [13] from the NetworkX package [39]. From the obtained graph, we use the node coordinates as the topographic layout of the neurons. For brevity, we refer to the co-activation graph technique as the "graph" method.

#### 3.2.3 Dimensionality Reduction

We test popular dimensionality reduction methods to project the high-dimensional neuron activation data into a lower-dimensional space while preserving most information.

<sup>1</sup><https://github.com/JustGlwing/minisom>



Principal Component Analysis (PCA) [12, 14, 15] is a traditional unsupervised technique for dimensionality reduction. The method linearly transforms the data points into a new coordinate system in which the new coordinates are the principal components, which are typically obtained from a Singular Value Decomposition (SVD) of the data matrix. We use the first and second principal component for projecting the data into two dimensions because these components describe the features of the highest explained variance. We use the PCA function from the decomposition module of Scikit-learn (sklearn) [37].

t-Distributed Stochastic Neighbor Embedding (tSNE) was first introduced by van der Maaten and Hinton [50]. Like PCA, tSNE is an unsupervised algorithm but the projection is non-linear. tSNE optimizes the pairwise similarities in the low-dimensional space to be similar to those in the original high-dimensional data using a cost function. We use the tSNE implementation from the sklearn manifold module. For stability of the tSNE algorithm, we initialize the learned embedding with PCA.

Uniform Manifold Approximation and Projection (UMAP) [30] is a recent non-linear dimensionality reduction algorithm. The authors claim that UMAP preserves the global structure better than tSNE. However, there is also counter-evidence by Kobak and Linderman [21] who showed that, given the same initialization, UMAP does not perform substantially better than tSNE. We create a two-dimensional UMAP projection with the python module umap-learn<sup>2</sup>.

### 3.2.4 Particle Swarm Optimization (PSO)

PSO [17, 42, 9] is a biologically inspired metaheuristic algorithm used to search for optimal solutions. It assigns each data point a particle in the solution space and searches the optimal solution by moving the particles based on simple mathematical formulas. Each individual particle follows simple local rules but many particles that influence each other create a complex structure. For our approach, we initialize a swarm of  $N$  particles in a two-dimensional solution space, where each particle corresponds to a neuron. With the PSO we aim to optimize two aspects that we encourage with designated update rules. First, similarly active neurons shall be in the vicinity of each other. Second, the neuron density shall be consistent in the layout, without gaps or clusters of neurons.

To achieve activation similarity of neighboring particles, we introduce a global force which is computed based on the actual neuron activation values. The global force encourages particles of similar neurons to attract each other while activation dissimilarity repels the corresponding particles:

$$f_{glob} = attr - rep \quad \text{with} \quad attr = a \cdot \left(1 - \frac{dist}{\max(dist)}\right)^3 \quad \text{and} \quad rep = b \cdot e^{-(dist/c)} \quad (1)$$

In Equation 1,  $f_{glob}$  = global force,  $attr$  = global attraction,  $rep$  = global repulsion,  $dist$  = Cosine distance matrix of the NAPs. For the global force, we set the weight parameters to  $a = 1.5, b = 0.5, c = 2$ .

To obtain a well-distributed layout, we use a local force that only depends on the particle coordinates. Like the global force, it consists of an attraction and a repulsion term. However, in the local force, attraction closes gaps in the layout by penalizing large distances between pairs of particles and repulsion avoids that two particles occupy the same position:

$$f_{loc} = attr - rep \quad \text{with} \quad attr = a \cdot \left(\frac{1}{(dist + 1)^3}\right) \quad \text{and} \quad rep = b \cdot e^{-(dist/c)} \quad (2)$$

In Equation 2,  $f_{loc}$  = local force,  $attr$  = local attraction,  $rep$  = local repulsion,  $dist$  = pairwise Euclidean distances between particles. The values that we use for the weight parameters of the local force are  $a = 1.5, b = 15, c = 2$ .

We optimize the PSO for  $T = 1000$  steps by updating the coordinates according to the weighted average of global and local force (Equation 3). In early steps  $t$ , we use a high global force weight  $w_g$  to encourage the activation similarity of neighboring particles and then gradually increase the local force weight  $w_l$  to better distribute the particles in the space.

$$f = \frac{1}{2} \cdot (w_g \cdot f_{glob} + w_l \cdot f_{loc}) \quad w_l(t) = \frac{1}{2} \cdot \left(\frac{e^{s(t)} - e^{-s(t)}}{e^{s(t)} + e^{-s(t)}} + 1\right) = 1 - w_g(t) \quad \text{with} \quad s(t) = \frac{9 \cdot t}{1000} - 3 \quad (3)$$

### 3.2.5 PSO with non-random initialization

The PSO method with random initialization needs careful balancing of the weight parameters of global and local attraction and repulsion. To require less fine-tuning of parameters, we investigate a variant of the PSO. Instead of optimizing the activation similarity with the global force, we compute an initial similarity-based layout with another method. We then only use the local force to further optimize the resulting layout with PSO. As the local force is

<sup>2</sup><https://github.com/lmcinnes/umap>

independent of the activation similarities, the PSO is only used to equally distribute the neurons in the two-dimensional space. We use the same parameters as for the PSO method with random initialization except for setting  $w_g = 0$  (Equation 3) in all optimization steps. Using either the UMAP, TSNE, graph, SOM or PCA method to initialize the PSO, we call the hybrid methods UMAP\_PSO, TSNE\_PSO, graph\_PSO, SOM\_PSO and PCA\_PSO.

### 3.3 Visualization

Finally, we use the NAP values (Section 3.1) and the layout coordinates (Section 3.2) to create topographic map images. To be able to compare different layouts, we first scale the layout coordinates such that in both dimensions the minimum value is 0 and the maximum value is 1 (Figure 1C). Then, we assign each layout coordinate a color according to the NAP value of the corresponding neuron for one group. We choose this color by mapping the NAP values to a symmetric continuous color scale, where blue represents  $-max(|NAP|)$ , white 0 and red  $+max(|NAP|)$ . Then, we linearly interpolate the colors with a resolution of  $100 \times 100$  px (Figure 1D). We use the same interpolation resolution for all methods because of the applied coordinate scaling. Equal colors in topographic maps of different groups represent the same NAP value, but the colors can correspond to different values in each experiment or layer.

## 4 Experimental Setup

This section describes the experiments that we perform to evaluate the quality of the topographic maps obtained with the proposed layouting methods. To select the technique with the best quality, we use a simple data set and a shallow model. In Section 6, we demonstrate that the selected method is also applicable to more complex models and data sets.

### 4.1 Data and Models

We first test our method with MNIST [24], a common benchmark data set for Machine Learning. MNIST contains grayscale images of handwritten digits from 0 to 9, which are of size  $28 \times 28$  px, centered and normalized in scale. There are 60,000 and 10,000 training and test data examples, respectively.

We train a simple MLP and CNN on the MNIST data set. The MLP has one fully-connected hidden layer of 128 neurons and uses Rectified Linear Unit (ReLU) [34] activation. The input images are flattened before providing them to the model. The CNN has two 2D-convolutional layers with kernel size  $3 \times 3$ , stride 2 and 128 filters, both using ReLU activation. The fully-connected classification layer takes the flattened feature maps of the second convolutional layer as input. During training, we use dropout and spatial dropout for fully-connected and convolutional layers, respectively, with a dropout rate of 0.5. An overview of the architectures is given in the Appendix Table 1. Both models are trained for 20 epochs using the Adam optimizer [20] with default parameters and categorical cross-entropy as the loss function.

### 4.2 Evaluation measures

**Qualitative criteria** Our technique aims to provide a comparative visual overview of the representations of groups in a DNN. The topographic maps are supposed to be easy to visually compare and they shall be perceived as similar to topographic maps in neuroscience. We consider the topographic maps to be visually similar to their neuroscientific inspiration if they have a round shape, contain no regions without neurons and show distinguishable regions of similar activity in all groups. To achieve comparability between topographic maps, they shall have a similar shape and size and they need to be discriminable for dissimilar groups. We qualitatively evaluate these expectations by manual inspection.

**Quantitative evaluation metrics** In addition to the manual inspection, we quantify the quality of the topographic maps. To test whether each position in a topographic map is similar to its neighborhood, we apply a Gaussian blur to the topographic map image and compute the Mean Squared Error (MSE) between the original and the blurred image. However, this metric penalizes boundaries between regions strongly, but clear boundaries can be beneficial to distinguish different regions from each other. Therefore, we use a second metric based on image resizing with bicubic interpolation because it preserves edges better than using Gaussian blur. For this metric, we downscale the images, upscale them to the original size again and compute the MSE between the upscaled and the original image. To not bias the quality metric based on the choice of a specific parameter, we compute the quality with different parameters for the radius of the Gaussian blur and the downscaling size. We use Gaussian blur with ten different radii, ranging from 2 px to 20 px in steps of 2 px and investigate ten different downscaling sizes for the original topomaps of size  $300 \times 300$  px from  $55 \times 55$  px down to  $10 \times 10$  px in steps of 5 px (see an example in Figure 2). To aggregate the results for the different parameter choices while interpolating the values for parameters in between, we use an estimated area under the curve (AUC) value. Using the parameters in the order of increasing effect of image alteration, we consider the resulting MSE values as function values and apply the trapezoidal rule with width 1 to estimate the AUC. Furthermore,

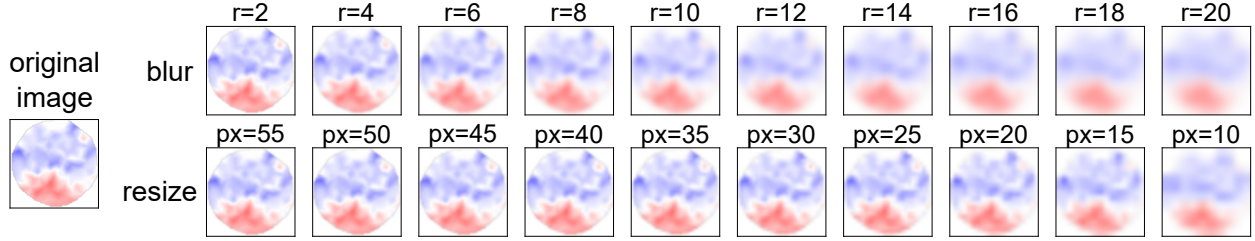


Figure 2: Examples of applying the blur and resize technique for quantifying topographic map quality with different Gaussian blur radii (top) and downscale sizes (bottom).

we investigate the robustness of the quality of the topographic maps. To this end, we repeat each topographic map computation 100 times given the same input. We also test whether the topographic map quality depends on the random choice of input examples for computing the NAPs by generating topographic maps for 100 resampled NAPs.

### 4.3 Experimental Plan

For our simplest data set and model, MNIST and MLP, we compute NAPs in the first fully-connected layer, using the 10 classes as grouping and 200 random examples per group. We then use the resulting NAPs to compute topographic maps with each of our 11 proposed layouting methods.

**Pre-selecting layouting methods** First, we pre-select a subset of techniques that satisfy the qualitative expectations of the visualization described in Section 4.2. For the exemplary class “0”, we compare the methods with respect to the formation of regions of similar activations, the visual similarity to a topographic map in neuroscience and the ease of comparability.

**Quantitative topographic map evaluation** Next, for the pre-selected methods, we investigate the quality of the resulting topographic maps in further detail. For each of the methods, we compute the quantitative evaluation measures described in Section 4.2 and compare the methods with respect to the visual quality of the topographic maps, the variation of the quality and the runtime. For CNNs, we use the complete feature map NAPs to compute the topographic map layouts but we aggregate the activation values per feature map to obtain a color for the topographic map. This difference to MLPs might affect which layouting method produces the best topographic maps. Therefore, we perform the same quantitative evaluation for a CNN model trained on MNIST. Based on the evaluation results for the MLP and the CNN, we pick the best method for the following experiments. In both evaluations, we include a random baseline layout to obtain an expected lower bound on the quality of the topographic maps. This random layout is a local force-only PSO which we initialize with random uniform values.

**Influence of NAP averaging** Finally, we evaluate whether the layouting methods require the NAP approach to perform well. A disadvantage of using NAPs as input to compute the layout is that it introduces weak supervision. In addition, the layout needs to be recomputed when changing the grouping. Being independent of the group information can potentially generalize our approach. Therefore, we investigate whether using a small random subset of the test data without averaging and normalization can approximate a layout of similar quality as with using NAPs. Specifically, we test two alternative ways to provide the inputs. As one alternative, we draw a random uniform number of examples of each class, such that the total number of examples adds up to 1000. This way, we simulate a data set with class imbalance and keep the number of examples the same as for computing the NAP. The second alternative input is to draw 200 random examples per class, but only stacking the activations instead of applying averaging and normalization across the groups.

## 5 Results and Discussion

### 5.1 Pre-selecting layouting methods

We first pre-select layouting methods that produce topographic maps which satisfy the qualitative criteria of Section 4.2. Topographic maps generated with each of the 11 methods for the MNIST MLP and the exemplary class “0” are shown in Figure 3. The Figure shows the topographic maps as scatter plots to see the positions of the neurons and potential gaps in the layout as well as the interpolated visualization as the final topographic maps. All methods are capable of distributing the neurons to form regions of similar activations. Only the SOM technique splits up sets of co-activated

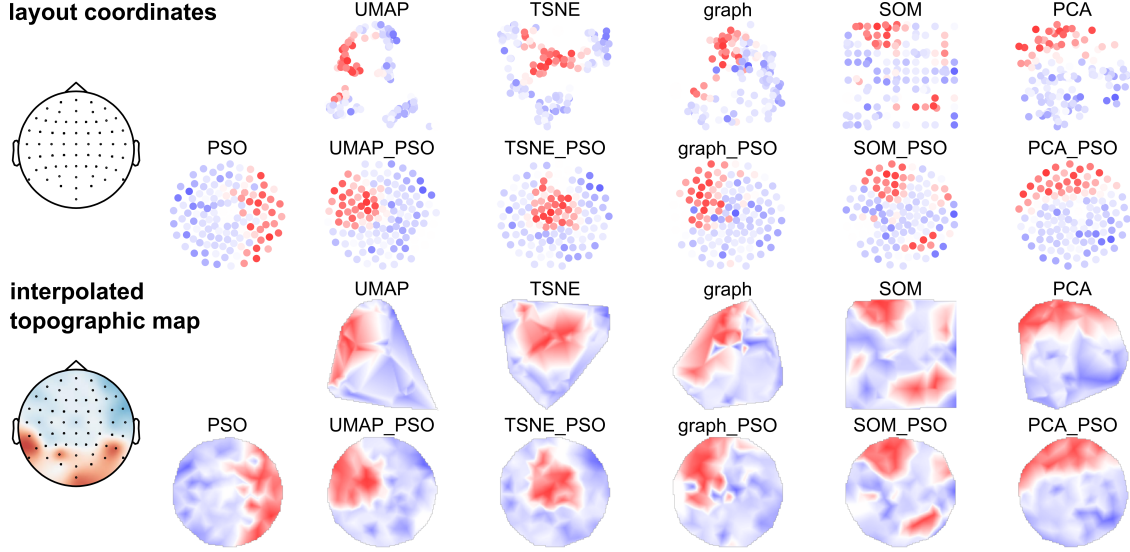


Figure 3: Topographic maps for one exemplary class for all proposed layouting methods. The scatter plots show the layouted neurons with NAP value-based coloring. Below are the resulting interpolated topographic maps. Left-most are examples of an electrode layout (top) and a topographic map (bottom) in neuroscience which we use as inspiration and qualitative target for our visualization. All layouts and colorings use the same class-based NAPs for an MNIST MLP model as input.

neurons into multiple regions in the layout. This can happen because a SOM does not penalize the similarity of distant coordinates, for example, when initializing two distant positions with similar neurons.

Another criterion is that the neurons are well-distributed in the two-dimensional space. One reason for this criterion is that there are no empty regions in a topographic map of a brain either. In addition, a layout with varying neuron density leads to disproportionated regions in the interpolated topographic maps. This effect can, for example, be observed in the TSNE topographic map. The region of highly active neurons in the center is surrounded by areas without assigned neurons. In the interpolated image, the gaps cause the red region to be enlarged, which wrongly suggests that the highly active neurons are in the majority for this class. We observe the strongest neuron density variation for UMAP and TSNE, and the graph method leads to high density for groups of co-activated neurons. With the SOM and PCA methods, the neurons are well-distributed in the shown example but a higher variation of the neuron density can happen for different data, models or parameters, too. The best distribution is achieved with the PSO method, which is almost free of gaps in the layout and the density of neurons is similar across the whole layout. This observation is not surprising because the PSO method optimizes this property of the layout with the local force component.

For the images to be visually similar to topographic maps in neuroscience, we expect them to have a round shape. This property is particularly well satisfied with the PSO method, regardless of the initialization, which is again achieved by the local force. However, when initializing the PSO randomly, the quality of the topographic map is unreliable. In the shown example of a PSO topographic map, we observe several neurons of low activity within regions of high activity. This effect is likely related to the simultaneous optimization of activation similarity and neuron distribution that can interfere with each other. This supports our idea of first layouting the neurons by activation similarity, followed by distributing the neurons with a PSO using the local force only. Therefore, we conclude that the PSO methods with non-random initialization are the most promising techniques. We will use these methods for the quantitative evaluation and keep the randomly initialized PSO for comparison, as well.

## 5.2 Quantitative Evaluation

For the methods that we pre-selected through qualitative evaluation, we further quantify their topographic map quality. The results for the first fully-connected layer of the MLP model trained on MNIST are shown in Figure 4A. Additionally, Figure 4C shows the corresponding runtimes of each method for different numbers of neurons. In MLPs, all methods obtain significantly better topographic maps than the random baseline layout. As expected, the PSO method with random initialization has the worst quality of results among the techniques, however, it is comparably as good as the PCA\_PSO technique. The quality of the PSO and PCA\_PSO methods mainly differ in their robustness across trials. While both have similar variations when using different random subsets per group as input, the PCA\_PSO layout quality

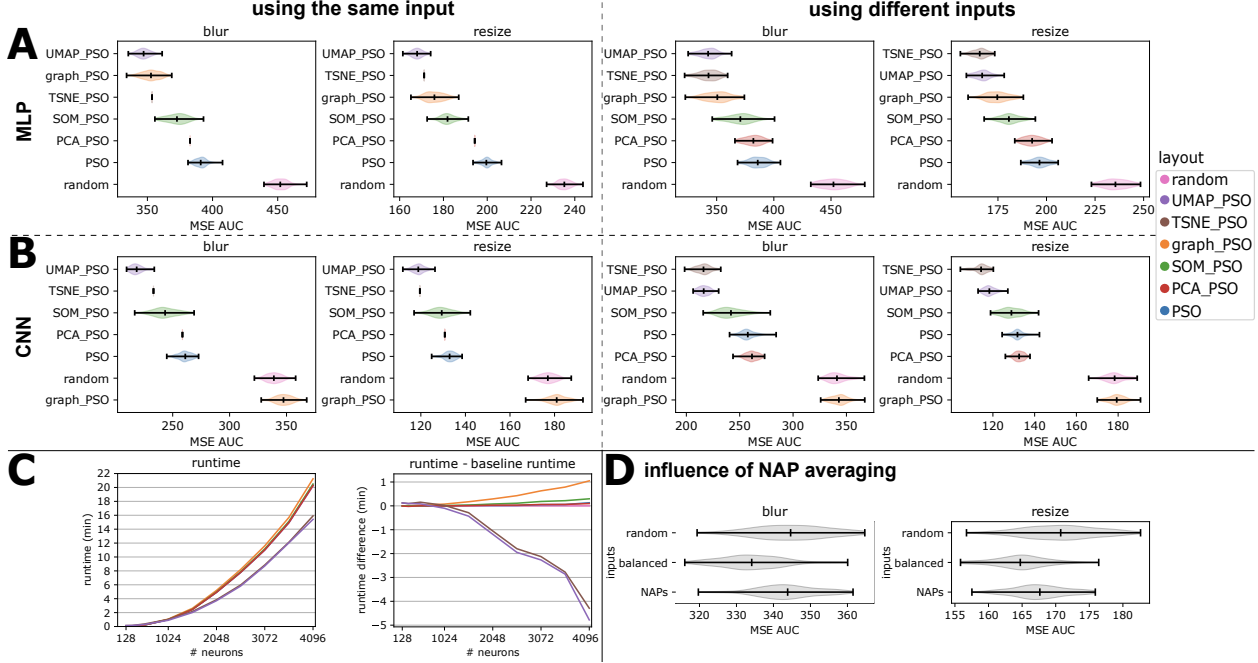


Figure 4: Quantification of the topographic map quality. Line plots: average quality values at each individual parameter of the evaluation measure. Violin plots: AUC value distributions across 100 trials, highlighting the mean AUC value and the extrema with markers. For A and B, the rows of each violin plot are sorted by the respective mean AUC values. Because AUC values are error values, the layouting methods are decreasing in quality from the top to the bottom row. C: Runtimes are mean values over 10 repeated computations per method and number of neurons. D: The averaging influence is investigated with UMAP\_PSO-based topographic maps using different strategies for computing activation distances between neurons. “random” and “balanced” pick 1000 random examples from the MNIST data set and use the concatenated activations of all examples. “balanced” additionally ensures that each group is represented equally often in the set. The “NAPs” approach further averages and normalizes the activations across each of the group.

is reproducible using the same input because PCA is a deterministic algorithm. SOM\_PSO and graph\_PSO are in the medium quality range. UMAP\_PSO and TSNE\_PSO obtain the highest quality results for the MLP according to both of the evaluation metrics. Like PCA\_PSO, TSNE\_PSO has a very small variation of quality when using the same inputs for computing the layout. This is because we use a TSNE algorithm that initializes the embedding positions with a PCA. Therefore, the result of TSNE\_PSO is robust although it is a stochastic algorithm. In the exemplary model layer with a small number of 128 neurons, UMAP\_PSO and TSNE\_PSO have a similar runtime. However, in wider layers with more neurons UMAP\_PSO is faster than TSNE\_PSO, for example, it needs around one minute less for a layer of 4096 neurons. Considering that we want to apply the same method to layers with any number of neurons, we conclude that UMAP\_PSO is the best layouting method.

**Applicability to CNNs** We perform the same experiment as for the MLP for an exemplary CNN model, as well. The results for the second convolutional layer of the CNN model are visualized in Figure 4B. We observe a major difference between MLP and CNN for the graph\_PSO method. For the CNN, the graph\_PSO is as low quality as the random baseline layout. This is due to the difficulty of choosing suitable parameters for creating the initial co-activation graph. The distance threshold used to create the graph in the MLP model is not suitable for the CNN model because of the change in the distribution of distance values. While this can be counteracted by optimizing the threshold value, it indicates that the graph\_PSO does not generalize well to different models. The findings for the remaining methods are comparable between MLP and CNN. UMAP\_PSO and TSNE\_PSO still produce results of similarly high quality. In the used CNN, TSNE\_PSO performs on average slightly better than UMAP\_PSO. However, the difference is neglectable and we argue that UMAP\_PSO is still the best choice taking the faster runtime for wider layers into account.

### 5.3 Influence of NAP averaging

Finally, using the UMAP\_PSO method and the MLP model, we investigate whether the averaging and normalizing of the NAP computation is necessary to achieve high-quality topographic maps. Figure 4D shows the quality value

distributions for the different ways of providing inputs to the layouting technique. “NAPs” indicates the default input we use in the previous section. Instead of applying averaging and normalization, we compare stacked random examples, either with a equal number of examples of each group (“balanced”) or with enforced class imbalance (“random”). The resulting layout quality of all three approaches does not differ substantially. Even with providing random examples without a balanced class distribution, the quality of the layout does not deteriorate much. This indicates that our approach allows to compute a topographic map layout without providing any information about the grouping.

We expected that using the NAPs as input leads to the best quality because the values for computing the layout are the same values as we used for the coloring. Surprisingly, drawing random examples with balanced group distribution performs slightly better than with NAPs as inputs. We suspect that the higher dimensionality when not averaging the activations provides more information for estimating the similarity of the neuron activations and therefore supports the layout computation. However, the higher dimensionality of the “balanced” approach also comes with higher computational requirements. This particularly limits its applicability for CNNs or fully-connected layers with a large number of neurons.

In conclusion of this experiment, all three tested approaches are useful. Picking random examples without information about the labels is suitable for unsupervised data or when testing different groupings with the same layout. A group-balanced random choice of examples produces the highest quality if it is computationally feasible. Using NAPs is the most generally applicable technique because it leads to high-quality topographic maps and scales well for complex models.

## 6 Exemplary Applications

For UMAP\_PSO, which we identified as the best layouting method in Section 5, we showcase exemplary use cases of our visualization. We demonstrate two toy applications to introduce how to use the visualization followed by a fairness application to show the real-world applicability of our technique.

### 6.1 Detecting systematic annotation errors in data sets

Topographic map visualizations can be used to identify whether classification errors are caused by wrong target annotations in the data set. Annotation errors can occur either in training data or test data which has different effects on the topographic maps. We demonstrate how to use our visualization technique for two toy examples, where we deliberately introduce annotation errors in either the training or test data.

#### 6.1.1 Toy examples design

For the first toy example, we use the Fashion MNIST data set [51] which is similar to MNIST. Both data sets contain the same number of training and test images, share a common image size and are grayscale. Fashion MNIST, in contrast, contains images of 10 different clothings or accessories which are more difficult object categories than handwritten digits. In the test data, we introduce a systematic error by changing the target class of 90% of the examples of class “0” (“T-shirt/Top”) to class “1” (“trouser”). Using this altered test data, we create topographic maps for a MLP model that is trained on the original Fashion MNIST training data. In the second toy example, we use the MNIST data set and introduce a systematic error in its training data. Specifically, we change 90% of the class “0” examples to class “1” and train a MLP model on this altered training data set. For this model, we create topographic maps for the original MNIST test data. Both toy examples only use the shallow MLP architecture as described in Section 4.1 and we use an unrealistically high amount of mislabeled examples to facilitate the understanding of the visualization. Nevertheless, both examples represent real-world scenarios that we discuss in the corresponding sections.

The groups of interest in both toy examples are the classes according to the test data annotations. Because we are further interested in the errors, we separate the examples of each class into whether they are correctly predicted by the model, resulting in 20 groups of interest. We create topographic maps for the first fully-connected layer of the respective MLP model using NAP values computed for 200 examples per group.

#### 6.1.2 Annotation errors in the test data

Figure 5 (top) shows the topographic maps of all Fashion MNIST classes, separated into correctly and wrongly classified groups. Two characteristics of the topographic maps indicate potential errors in the annotation of the test data. First, erroneous test data annotations lead to a high difference of the activity between the topographic maps of correctly and wrongly classified examples of the same label. Second, the activity of the wrongly classified group is similar to the activity of another group, that is, the class which the examples are supposed to be annotated as. In the shown example,



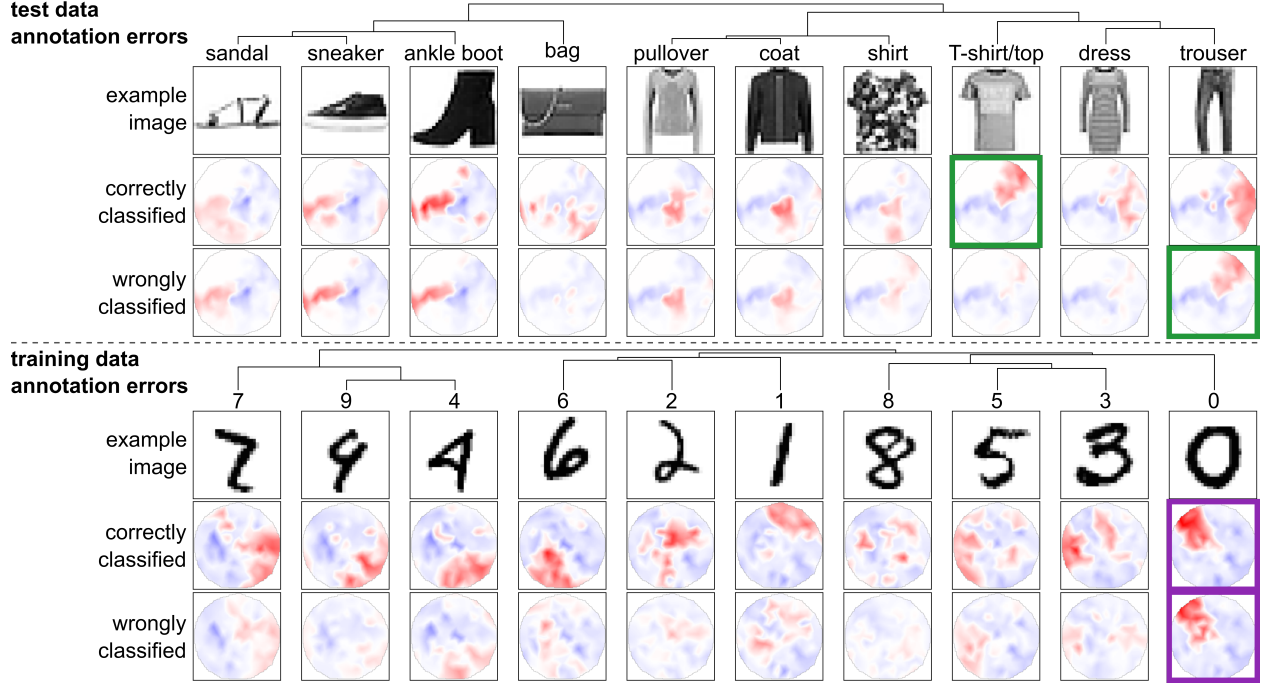


Figure 5: Topographic maps for correctly and wrongly classified examples using data sets with annotation errors. Top: annotation errors in the test data. Bottom: training data with annotation errors. The activation similarity is shown as a dendrogram and used to sort the classes. The shown example images are randomly chosen from the respective group, while 200 examples per group are used to compute the NAP. The green and purple annotations highlight the pairs of topographic maps that indicate the error in the respective example.

the first criterion is met for several classes, for example, “bag”, “T-shirt/top” and “trouser”. Only for the wrongly classified “trouser” group, we observe that the topographic map is similar to the activation of correctly classified “T-shirt/top” images (highlighted in green). This matches the error that we injected in the test data, that is, changing 90% of the “T-shirt/top” labels to “trouser”.

In realistic models, a dissimilarity between the topographic maps of the correctly and wrongly classified groups of the same annotation indicates that there is a distribution difference in this class. If no other topographic map is similar, this low similarity can be related to using non-representative training data for this class or using test data with a highly different distribution. The model can potentially be improved by including a part of the out-of-distribution examples in the training data or by introducing a new class which represents them.

In the upper left of the topographic maps in Figure 5 (top), we observe a white region in all groups. This region is not empty because the PSO distributes the neurons in a round shape. Instead, a white region that exists in all groups corresponds to a larger subset of neurons whose activity is highly similar across the groups. This indicates that the model is not using its full capacity, for example, because it is too complex for the given task or due to training problems like ReLUs that never activate [27].

### 6.1.3 Annotation errors in the training data

To investigate training data annotation errors, we train a model using an erroneous MNIST data set. The resulting topographic maps of correctly and wrongly classified groups using the original MNIST data set are shown in Figure 5 (bottom). Like in the previous example, we visually compare the topographic maps to identify potential errors in the training data. However, the criteria are different from the ones for the test data. Annotation errors in the training data lead to a high similarity of topographic maps for wrongly and correctly classified examples of the same group. This means that the model detects similar patterns in both groups but still categorizes the examples differently, which indicates an error in the classification decision that is based on the training data annotations. In addition, there is typically no other topographic map that is highly similar to the potential error candidate. We observe this pattern for class “0” (purple highlight), which again matches our injected annotation error of changing 90% of the “0” labels. However, using the binary split into correctly and wrongly classified examples does not show which class the training examples

are mislabeled as. To identify the class of the wrong annotations, we can extend the analysis by creating a confusion matrix-like topographic maps visualization. There, we can find that the topographic map at the “0”-classified-as-“1” position is highly similar to the correctly classified “0” examples (see Appendix Figure 7).

Observing similar topographic maps of the correctly and wrongly classified examples of the same class can also give insight in realistic models. Commonly, this pattern occurs if the model cannot discriminate between two or more classes properly. In this case, there are multiple classes that share similar topographic maps in the correctly and wrongly classified groups. One example can be found in the classes “sneaker” and “ankle boot” of Figure 5 (top). There are no changes in the annotations of these two classes but the topographic maps of the corresponding groups look similar. This indicates that the classes are too similar to each other for the model to discriminate between them. Improvements of the model can be achieved by merging the classes that are similar to each other or by increasing the model capacity to strengthen its ability to distinguish between the similar classes.

## 6.2 Visualization of bias in representations

As a real-world example, we investigate the bias in the representations in VGG16 [43], which is a pre-trained CNN model that is commonly used as feature extractor for downstream applications like image recognition DNNs. As test data, we use FairFace [16], a balanced data set of images of people from different age groups, races and binary genders. Here, we choose the “race” variable as grouping to compute the topographic maps. Moreover, as a random baseline to compare with, we add several groups of randomly picked examples. We investigate the representations of a pre-trained VGG16 model, obtained from the TensorFlow Keras applications<sup>3</sup> module, using the second maxpooling layer as an example. In the appendix, we provide the VGG16 architecture (Table 1) and topographic maps of multiple layers of the network (Figure 8).

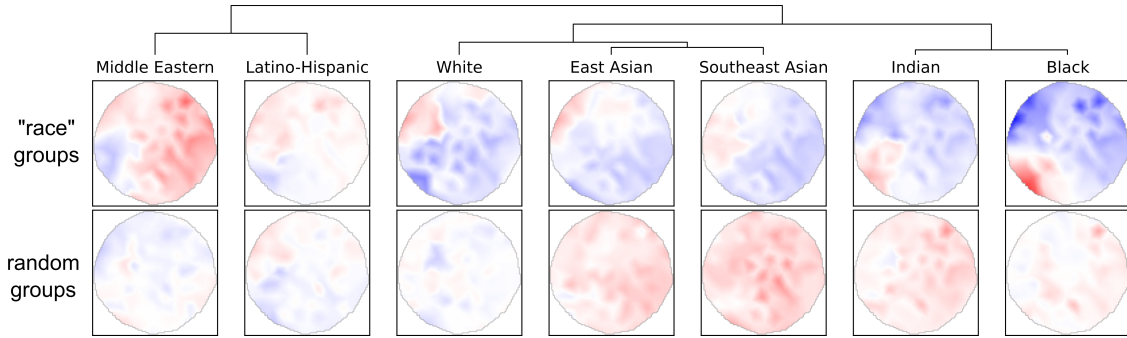


Figure 6: Topographic maps of VGG16 activations in the second maxpooling layer for different FairFace “race” categories (top) and random groups (bottom). In each row, the groups are sorted by activation similarity.

By comparing the topographic maps between the values of the sensitive variables from FairFace, we investigate whether it is possible to visually discriminate the groups based on the representations of the VGG16 model. If the topographic maps of the bias variable categories are easier to discriminate than topographic maps of random groups, we consider the representations to be biased. Figure 6 shows the topographic maps for the seven “race” categories of the FairFace data set and of seven random groups in the second maxpooling layer of the VGG16 model. First, we observe that it is clearly easier to discriminate the “race” categories than the random groups. The topographic maps of the “race” categories show distinct regions of highly and weakly active neurons and are of higher contrast and color intensity than those of the random groups. This indicates that the representations are biased towards the “race” variable. Only the “Latino-Hispanic” topographic map can be confused with a random group, either because the input images or the model representations for this category are too heterogeneous. We further observe that “Indian” and “Black” are perceived as particularly similar by the model. “East Asian” and “Southeast Asian” are similar to each other and to the “White” category. “Middle Eastern” and “Latino-Hispanic” are dissimilar to the other groups.

Because the representations are visually discriminable, they will likely affect downstream applications using the pre-trained model. For example, a classifier that uses these pre-trained representations can easily learn different decisions for the “White” and “Black” categories because their representations differ substantially. We emphasize, however, that this observation does not imply that a downstream application must include a racial bias. Instead, we suggest to use the findings from the visualization to formulate hypotheses about which bias to look for. In this specific case, the topographic map visualization indicates that there is a higher risk for learning a biased decision between the “White”

<sup>3</sup><https://github.com/keras-team/keras>



and “Black” category. Further, the observations indicate that there might be unintended correlations of the decisions for the representationally similar categories “Indian” and “Black” or “East Asian“, “Southeast Asian“ and “White”. This allows to test for biases in a targeted way instead of running a computationally expensive test for all potential biases.

## 7 Conclusion

Topographic activation maps are a promising visualization tool to get insight into the internal representations of DNNs. Our technique simplifies high-dimensional neural activity in a hidden layer of the DNN model into a two-dimensional visualization. This allows to obtain a graphical overview that can be used to visually compare DNN representations between groups of interest without being restricted to using only the output classes of the model.

Our visualization technique alone does not explicitly provide explanations of the model representations or decisions. It still requires a human to visually interpret the results or to perform further downstream analyses, like computing feature visualization or saliency maps, to explain what the regions are responsible for. While topographic maps are easy to interpret by visual inspection, relating the visualization to useful insight into the model requires some practice, especially for highly-complex models that are used in practical applications. We therefore recommend to first get familiar with the technique by using toy examples before applying it to real-world models.

In future research, we will investigate how to generate explanations of the regions in our topographic map visualization. For example, we will automatically detect group-responsive regions and perform feature visualization for the corresponding filters of the model to understand which patterns it uses to detect the respective group. Moreover, we will research extensions of our technique to create topographic map visualizations that span multiple layers.

## Acknowledgments

This research has been funded by the Federal Ministry of Education and Research of Germany (BMBF) as part of the project “CogXAI–Cognitive neuroscience inspired techniques for eXplainable AI”.

## References

- [1] Julius Adebayo, Justin Gilmer, Michael Muelly, Ian Goodfellow, Moritz Hardt, and Been Kim. Sanity checks for saliency maps. In *Advances in Neural Information Processing Systems*, pages 9525–9536, 2018.
- [2] Jaimeen Ahn and Alice Oh. Mitigating language-dependent ethnic bias in BERT. In *Proceedings of the Conference on Empirical Methods in Natural Language Processing (EMNLP)*, pages 533–549, Online and Punta Cana, Dominican Republic, November 2021. Association for Computational Linguistics.
- [3] Guillaume Alain and Yoshua Bengio. Understanding intermediate layers using linear classifier probes. In *International Conference on Learning Representations (ICLR), Workshop Track Proceedings*, 2017.
- [4] Sebastian Bach, Alexander Binder, Grégoire Montavon, Frederick Klauschen, Klaus-Robert Müller, and Wojciech Samek. On pixel-wise explanations for non-linear classifier decisions by layer-wise relevance propagation. volume 10, page e0130140. Public Library of Science, 2015.
- [5] Sören Becker, Marcel Ackermann, Sebastian Lapuschkin, Klaus-Robert Müller, and Wojciech Samek. Interpreting and explaining deep neural networks for classification of audio signals. 2018.
- [6] Tolga Bolukbasi, Kai-Wei Chang, James Y Zou, Venkatesh Saligrama, and Adam T Kalai. Man is to computer programmer as woman is to homemaker? debiasing word embeddings. volume 29, pages 4349–4357, 2016.
- [7] Joy Buolamwini and Timnit Gebru. Gender shades: Intersectional accuracy disparities in commercial gender classification. In Sorelle A. Friedler and Christo Wilson, editors, *Proceedings of the 1st Conference on Fairness, Accountability and Transparency*, volume 81, pages 77–91. PMLR, 23–24 Feb 2018.
- [8] Jacob Devlin, Ming-Wei Chang, Kenton Lee, and Kristina Toutanova. Bert: Pre-training of deep bidirectional transformers for language understanding. 2019.
- [9] R.C. Eberhart and Y. Shi. Comparing inertia weights and constriction factors in particle swarm optimization. In *Proceedings of the Congress on Evolutionary Computation.*, volume 1, pages 84–88 vol.1, 2000.
- [10] Dumitru Erhan, Yoshua Bengio, Aaron Courville, and Pascal Vincent. Visualizing higher-layer features of a deep network. volume 1341, page 1, 2009.
- [11] James Fiocco, Samridhi Choudhary, and Carolyn Rose. Deep neural model inspection and comparison via functional neuron pathways. In *Annual Meeting of the Association for Computational Linguistics (ACL)*, pages 5754–5764, 2019.

- [12] Karl Pearson F.R.S. On lines and planes of closest fit to systems of points in space. volume 2, pages 559–572. Taylor & Francis, 1901.
- [13] Thomas MJ Fruchterman and Edward M Reingold. Graph drawing by force-directed placement. volume 21, pages 1129–1164. Wiley Online Library, 1991.
- [14] Harold Hotelling. Analysis of a complex of statistical variables into principal components. volume 24, pages 498–520, 1933.
- [15] Ian Jolliffe. *Principal Component Analysis*. Springer Verlag, New York, 2002.
- [16] Kimmo Karkkainen and Jungseock Joo. Fairface: Face attribute dataset for balanced race, gender, and age for bias measurement and mitigation. In *Proceedings of the IEEE/CVF Winter Conference on Applications of Computer Vision*, pages 1548–1558, 2021.
- [17] J. Kennedy and R. Eberhart. Particle swarm optimization. In *Proceedings of International Conference on Neural Networks (ICNN)*, volume 4, pages 1942–1948 vol.4, 1995.
- [18] Been Kim, Martin Wattenberg, Justin Gilmer, Carrie Cai, James Wexler, Fernanda Viegas, et al. Interpretability beyond feature attribution: Quantitative testing with concept activation vectors (tcav). In *International Conference on Machine Learning (ICML)*, pages 2668–2677, 2018.
- [19] Pieter-Jan Kindermans, Kristof T. Schütt, Maximilian Alber, Klaus-Robert Müller, Dumitru Erhan, Been Kim, and Sven Dähne. Learning how to explain neural networks: Patternnet and patternattribution. In *International Conference on Learning Representations (ICLR)*, 2018.
- [20] Diederik P Kingma and Jimmy Ba. Adam: A method for stochastic optimization. 2014.
- [21] Dmitry Kobak and George C. Linderman. Umap does not preserve global structure any better than t-sne when using the same initialization. Cold Spring Harbor Laboratory, 2019.
- [22] Teuvo Kohonen. *Self-Organizing Feature Maps*, pages 119–157. Springer Berlin Heidelberg, Berlin, Heidelberg, 1988. ISBN 978-3-662-00784-6.
- [23] Andreas Krug, Maral Ebrahimzadeh, Jost Alemann, Jens Johansmeier, and Sebastian Stober. Analyzing and visualizing deep neural networks for speech recognition with saliency-adjusted neuron activation profiles. volume 10, page 1350. Multidisciplinary Digital Publishing Institute, 2021.
- [24] Yann LeCun and Corinna Cortes. MNIST handwritten digit database. 2010.
- [25] Bingbing Li, Hongwu Peng, Rajat Sainju, Junhuan Yang, Lei Yang, Yueying Liang, Weiwen Jiang, Binghui Wang, Hang Liu, and Caiwen Ding. Detecting gender bias in transformer-based models: A case study on bert. 2021.
- [26] Nan Liu, Jinjun Wang, and Yihong Gong. Deep self-organizing map for visual classification. In *International Joint Conference on Neural Networks (IJCNN)*, pages 1–6. IEEE, 2015.
- [27] Andrew L Maas, Awni Y Hannun, Andrew Y Ng, et al. Rectifier nonlinearities improve neural network acoustic models. In *International Conference on Machine Learning (ICML)*, volume 30, page 3. Citeseer, 2013.
- [28] Scott Makeig, Julie Onton, et al. ERP features and EEG dynamics: an ICA perspective. In *Oxford handbook of event-related potential components*, pages 51–87. Oxford, 2009.
- [29] Konrad Maurer and Thomas Dierks. *Atlas of Brain Mapping: Topographic Mapping of EEG and Evoked Potentials*. Springer Science & Business Media, 2012.
- [30] Leland McInnes, John Healy, and James Melville. Umap: Uniform manifold approximation and projection for dimension reduction. 2020.
- [31] Ari S Morcos, Maithra Raghu, and Samy Bengio. Insights on representational similarity in neural networks with canonical correlation. 2018.
- [32] Alexander Mordvintsev, Christopher Olah, and Mike Tyka. Inceptionism: Going deeper into neural networks. volume 20, page 5, 2015.
- [33] Tasha Nagamine, Michael L Seltzer, and Nima Mesgarani. Exploring how deep neural networks form phonemic categories. In *Sixteenth Annual Conference of the International Speech Communication Association*, 2015.
- [34] Vinod Nair and Geoffrey E Hinton. Rectified linear units improve restricted boltzmann machines. In *International Conference on Machine Learning (ICML)*, pages 807–814, 2010.
- [35] Weili Nie, Yang Zhang, and Ankit Patel. A theoretical explanation for perplexing behaviors of backpropagation-based visualizations. In *International Conference on Machine Learning (ICML)*, pages 3809–3818, 2018.
- [36] Simon Osindero and Geoffrey E Hinton. Modeling image patches with a directed hierarchy of markov random fields. In *Advances in Neural Information Processing Systems*, pages 1121–1128, 2008.

- [37] Fabian Pedregosa, Gaël Varoquaux, Alexandre Gramfort, Vincent Michel, Bertrand Thirion, Olivier Grisel, Mathieu Blondel, Peter Prettenhofer, Ron Weiss, Vincent Dubourg, et al. Scikit-learn: Machine learning in python. volume 12, pages 2825–2830. JMLR. org, 2011.
- [38] Lauréline Perotin, Romain Serizel, Emmanuel Vincent, and Alexandre Guérin. Crnn-based multiple doa estimation using acoustic intensity features for ambisonics recordings. volume 13, pages 22–33. IEEE, 2019.
- [39] Daniel A Schult. Exploring network structure, dynamics, and function using networkx. In *In Proceedings of the 7th Python in Science Conference (SciPy)*. Citeseer, 2008.
- [40] Karl Schulz, Leon Sixt, Federico Tombari, and Tim Landgraf. Restricting the flow: Information bottlenecks for attribution. In *International Conference on Learning Representations (ICLR)*, 2019.
- [41] Ramprasaath R Selvaraju, Michael Cogswell, Abhishek Das, Ramakrishna Vedantam, Devi Parikh, and Dhruv Batra. Grad-cam: Visual explanations from deep networks via gradient-based localization. In *IEEE International Conference on Computer Vision (ICCV)*, pages 618–626, 2017.
- [42] Y. Shi and R. Eberhart. A modified particle swarm optimizer. In *IEEE International Conference on Evolutionary Computation Proceedings.*, pages 69–73, 1998.
- [43] Karen Simonyan and Andrew Zisserman. Very deep convolutional networks for large-scale image recognition. 2014.
- [44] Karen Simonyan, Andrea Vedaldi, and Andrew Zisserman. Deep inside convolutional networks: Visualising image classification models and saliency maps. 2013.
- [45] Leon Sixt, Maximilian Granz, and Tim Landgraf. When explanations lie: Why many modified bp attributions fail. In *International Conference on Machine Learning (ICML)*, pages 9046–9057, 2020.
- [46] Jost Tobias Springenberg, Alexey Dosovitskiy, Thomas Brox, and Martin Riedmiller. Striving for simplicity: The all convolutional net. 2014.
- [47] Latanya Sweeney. Discrimination in online ad delivery. 2013.
- [48] Christian Szegedy, Wei Liu, Yangqing Jia, Pierre Sermanet, Scott Reed, Dragomir Anguelov, Dumitru Erhan, Vincent Vanhoucke, and Andrew Rabinovich. Going deeper with convolutions. In *IEEE Conference on Computer Vision and Pattern Recognition (CVPR)*, pages 1–9, 2015.
- [49] Etienne Thuillier, Hannes Gamper, and Ivan J Tashev. Spatial audio feature discovery with convolutional neural networks. In *IEEE International Conference on Acoustics, Speech and Signal Processing (ICASSP)*, pages 6797–6801, 2018.
- [50] Laurens van der Maaten and Geoffrey Hinton. Visualizing data using t-sne. volume 9, pages 2579–2605, 2008.
- [51] Han Xiao, Kashif Rasul, and Roland Vollgraf. Fashion-MNIST: a novel image dataset for benchmarking machine learning algorithms. 2017.
- [52] Jason Yosinski, Jeff Clune, Anh Nguyen, Thomas Fuchs, and Hod Lipson. Understanding neural networks through deep visualization. 2015.
- [53] Matthew D Zeiler and Rob Fergus. Visualizing and understanding convolutional networks. In *European Conference on Computer Vision (ECCV)*, pages 818–833. Springer, 2014.

## Appendix

## A1 Confusion matrix-like topographic map visualization



Figure 7: Topographic maps for correctly and wrongly classified examples, with the misclassification groups further split by the predicted label. The examples are based on a toy example model trained on data with annotation errors. The MNIST images in the top row and left-most column are an exemplary input of the respective group, while 200 examples were used to compute each NAP. Empty topographic maps indicate that the corresponding wrong classification was not made by the model. The purple annotation highlights the pair of topographic maps to identify the error in the toy example.

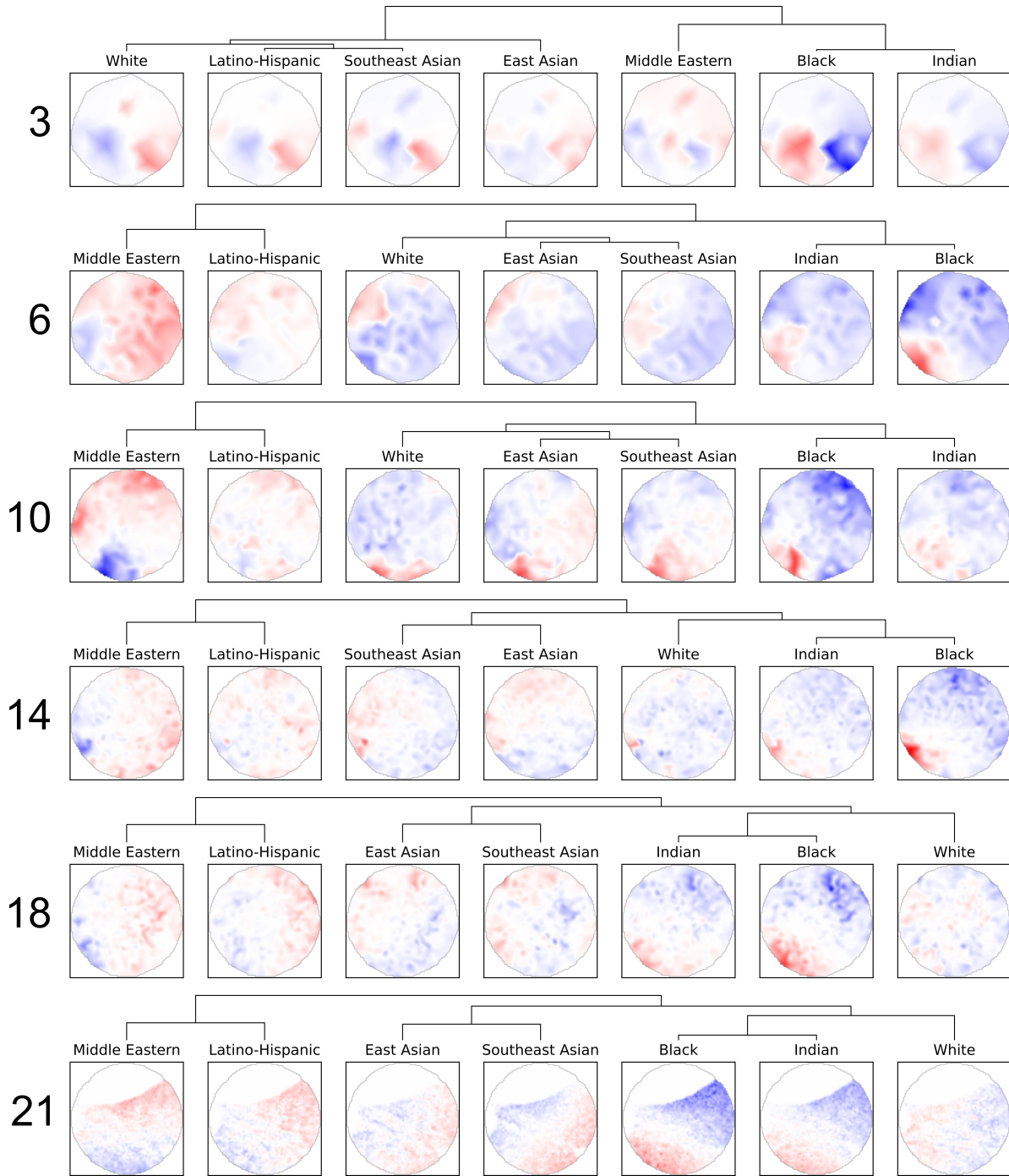
**A2 VGG16 topographic maps in different layers**

Figure 8: Topographic maps of VGG16 activations in all maxpooling layers (layers 3, 6, 10, 14, 18) and the last fully-connected layer (layer 21) for the FairFace "race" categories. The groups of each row are sorted by their activation similarity.

### A3 Model architectures

Table 1: Architecture details of the MLP, CNN and VGG16 models. The respective layers for creating the topographic map visualizations in the Sections 5 and 6 are highlighted in bold print.

model	layer	kernel size	stride	padding	neurons/ filters	output shape	params	activation
<b>MLP</b>	Flatten					784	0	
	<b>Fully-Connected</b>				<b>128</b>	<b>128</b>	<b>100,480</b>	<b>ReLU</b>
	Fully-Connected				10	10	1,290	Softmax
							$\Sigma = 101,770$	
<b>CNN</b>	Conv2D	$3 \times 3$	2	valid	128	$13 \times 13 \times 128$	1280	ReLU
	<b>Conv2D</b>	$3 \times 3$	<b>2</b>	valid	<b>128</b>	<b><math>6 \times 6 \times 128</math></b>	<b>147,584</b>	<b>ReLU</b>
	Flatten					4,608	0	
	Fully-Connected				10	10	46,090	Softmax
							$\Sigma = 194,954$	
<b>VGG16</b>	Conv2D	$3 \times 3$	1	same	64	$224 \times 224 \times 64$	1,792	ReLU
	Conv2D	$3 \times 3$	1	same	64	$224 \times 224 \times 64$	36,928	ReLU
	3 MaxPooling2D	$2 \times 2$	2	valid		$112 \times 112 \times 64$	0	
	Conv2D	$3 \times 3$	1	same	128	$112 \times 112 \times 128$	73,856	ReLU
	Conv2D	$3 \times 3$	1	same	128	$112 \times 112 \times 128$	147,584	ReLU
	<b>6 MaxPooling2D</b>	$2 \times 2$	<b>2</b>	<b>valid</b>		<b><math>56 \times 56 \times 128</math></b>	<b>0</b>	
	Conv2D	$3 \times 3$	1	same	256	$56 \times 56 \times 256$	295,168	ReLU
	Conv2D	$3 \times 3$	1	same	256	$56 \times 56 \times 256$	590,080	ReLU
	Conv2D	$3 \times 3$	1	same	256	$56 \times 56 \times 256$	590,080	ReLU
	10 MaxPooling2D	$2 \times 2$	2	valid		$28 \times 28 \times 256$	0	
	Conv2D	$3 \times 3$	1	same	512	$28 \times 28 \times 512$	1,180,160	ReLU
	Conv2D	$3 \times 3$	1	same	512	$28 \times 28 \times 512$	2,359,808	ReLU
	Conv2D	$3 \times 3$	1	same	512	$28 \times 28 \times 512$	2,359,808	ReLU
	14 MaxPooling2D	$2 \times 2$	2	valid		$14 \times 14 \times 512$	0	
	Conv2D	$3 \times 3$	1	same	512	$14 \times 14 \times 512$	2,359,808	ReLU
	Conv2D	$3 \times 3$	1	same	512	$14 \times 14 \times 512$	2,359,808	ReLU
	Conv2D	$3 \times 3$	1	same	512	$14 \times 14 \times 512$	2,359,808	ReLU
	18 MaxPooling2D	$2 \times 2$	2	valid		$7 \times 7 \times 512$	0	
	Flatten					25088	0	
	Fully-Connected				4096	4096	102,764,544	ReLU
	21 Fully-Connected				4096	4096	16,781,312	ReLU
	Fully-Connected				1000	1000	4,097,000	Softmax
							$\Sigma = 138,357,544$	